RSC Advances

ROYAL SOCIETY OF CHEMISTRY

www.rsc.org/advances

Modulating Hierarchical Self-Assembly Behavior of Peptide Amphiphile/Nonionic Surfactant Mixed System

Han Zhang [a †], Menghong Yu [a †], Aixin Song [a], Yawen Song [a], Xia Xin [a, b *], Jinglin Shen [a], Shiling Yuan [a *]

[a] *Key Laboratory of Colloid and Interface Chemistry (Shandong University), Ministry of Education, Shanda nanlu No. 27, Jinan, 250100, P. R. China*

[b] *National Engineering Technology Research Center for Colloidal Materials, Shandong University, Shanda nanlu No. 27, Jinan, 250100, P. R. China*

* Author to whom correspondence should be addressed, E-mail: xinx@sdu.edu.cn.

Phone: +86-531-88363597. Fax: +86-531-88361008

* Author to whom correspondence should be addressed, E-mail: shilingyuan@sdu.edu.cn.

Phone: +86-531-88365896. Fax: +86-531-88564750

† H. Zhang and M. H. Yu contributed equally.

Abstract

The self-assembly behavior of a nonionic surfactant (n-dodecyl tetraethylene monoether, $C_{12}E_4$) and a peptide amphiphile (PA, C_{16}-GK-3) mixed system were investigated using a combination of microscopic, scattering and spectroscopic techniques including transmission electron microscopy (TEM), field emission-scanning electron microscopy (FE-SEM), atomic force microscopy (AFM), polarized optical microscopy (POM) observations, small-angle X-ray scattering (SAXS), Fourier transform infrared (FT-IR), circular dichroism (CD) and rheological measurements. With the change of the contents of C_{16}-GK-3 and $C_{12}E_4$, it induced the transitions in the nanostructures and simultaneously led to changes in macroscopic properties, that is, mixtures of $C_{12}E_4$ with C_{16}-GK-3 can be hierarchically self-assembled into various helical nanofibers and then further assembled to dandelion-like and dendrite nanostructures by changing the composition of C_{16}-GK-3 and $C_{12}E_4$ which resulted transitions from solution, two phase, sol to hydrogel state were noted on the increasing the concentration of C_{16}-GK-3 at a fixed concentration of $C_{12}E_4$ or varying $C_{12}E_4$ concentration at a fixed concentration of C_{16}-GK-3. On the basis of a series of characterizations, we proposed the possible mechanism of the self-assembly, for which the hydrogen bonding interaction between the headgroups of C_{16}-GK-3 and between C_{16}-GK-3 and $C_{12}E_4$ as well as hydrophobic interaction between the alkyl chains of C_{16}-GK-3 and $C_{12}E_4$ were the main driving forces.

Introduction

Under the environment of vigorously promoting the environmental protection and development of green chemistry, the study of peptide amphiphiles (PAs) becomes a hot topic and have attracted much attention [1-4]. PAs are a class of molecules that normally consist of a hydrophobic alkyl tail

or lipid chain with the functions of bioactive hydrophilic peptide sequence which induces them to have amphiphilicity and promotes their self-assembly behavior [5-8]. Thus, PAs are known to assemble into a variety of nanostructures such as micelles, vesicles, nanotubes, nanorods, nanobelts, nanoribbons, and nanofibers in different solvents or under certain conditions such as pH, temperature and ionic strength [9-15]. The self-assembly process is controlled by many factors including hydrophobic interactions, electrostatic interactions, inter- or intramolecular hydrogen bonds, and van der Waals forces [16-18]. Because of its rich self-assembling behavior and its biocompatibility, PAs have wide applications in the field of biomaterials and nanomedicine, including tissue engineering, 3D cell culture, regenerative medicine, bacteria inhibition and drug delivery [19-25].

In general, the peptide amphiphiles have biologically relevant lipid chain lengths, in particular palmitoyl (hexadecyl, C_{16}) [26]. For example, Hest et al. have investigated the influence of mono-alkyl chain length on the self-assembly of PAs containing an octapeptide derived from a protein of the malaria parasite P. falciparum. The results indicated that short chains (C_6–C_{12}) can only produce random coil structures, while β-sheet ordering structure was only observed for C_{14} and C_{16} derivatives and the C_{16} variant showed the most extended thermal stability range for β-sheet structure [27]. Hotta et al. have discussed the effects of the salt concentrations using sodium dihydrogenorthophosphate (NaH_2PO_4) on the sol-gel transition behaviors, especially the gelation speed and the gel characteristics of the designed PA (C_{16}-W3K) hydrogels in aqueous solution. Their results indicated that the solution exhibited higher gelation speeds and higher mechanical properties at higher salt concentrations and concurrently, the density, the length of wormlike micelles, and the conformational ratio of β-sheets to α-helices in the equilibrium C_{16}-W3K solutions

all increased with the increase in the salt concentrations [28]. Moreover, the study of the interaction between traditional surfactant and PAs can rich the phase behaviors and self-assembly structures of PAs. For example, Hamley et al. have investigated the self-assembly of Pluronic copolymer P123 with the PA C_{16}-KTTKS. The results revealed that the β-sheet structure of C_{16}-KTTKS is retained even with 20 wt% added P123 and the nanotapes comprising peptide bilayers observed for C_{16}-KTTKS itself in aqueous solution are progressively replaced by cylindrical fibrils upon addition of more P123 [29]. They have also studied the interaction between the classical anionic surfactant sodium dodecyl sulfate (SDS) and C_{16}-KTTKS. The results indicated that the addition of SDS leads to a transition from tapes to fibrils, via intermediate states that include twisted ribbons and the addition of SDS is also shown to enhance the development of remarkable lateral ‘‘stripes’’ on the nanostructures which is ascribed to counterion condensation [30].

In this article, the binding of a nonionic surfactant (n-dodecyl tetraethylene monoether, $C_{12}E_4$) to a PA C_{16}-GK-3 containing a cationic peptide headgroup and its effects on the self-assembly behavior of $C_{12}E_4$/C_{16}-GK-3 mixed systems were investigated. Transmission electron microscopy (TEM), field emission-scanning electron microscopy (FE-SEM), atomic force microscopy (AFM), polarized optical microscopy (POM) observations, small-angle X-ray scattering (SAXS), Fourier transform infrared (FT-IR), circular dichroism (CD) and rheological measurements were used to characterize their physicochemical properties. Our aim is to examine the influence of uncharged surfactant $C_{12}E_4$ on the aggregation of C_{16}-GK-3 in aqueous solutions to increase and enrich the examples of interactions between peptides and surfactants.

Experimental

Chemicals

Nonionic surfactant ($C_{12}E_4$) was purchased from Acros Organics (USA) and the purity was greater than 99%. C_{16}-GK-3 (98%) was purchased from GL Biochem (Shanghai) Ltd. and used without further purification. The C_{16}-GK-3 (pI = 8.94) molecule is a 3-amino acid chain composed of glycine, histidine, lysine attached to a 16-carbon alkyl tail (Figure 1). All the above reagents were used without further purification. Water used in the experiments was triply distilled using a quartz water purification system.

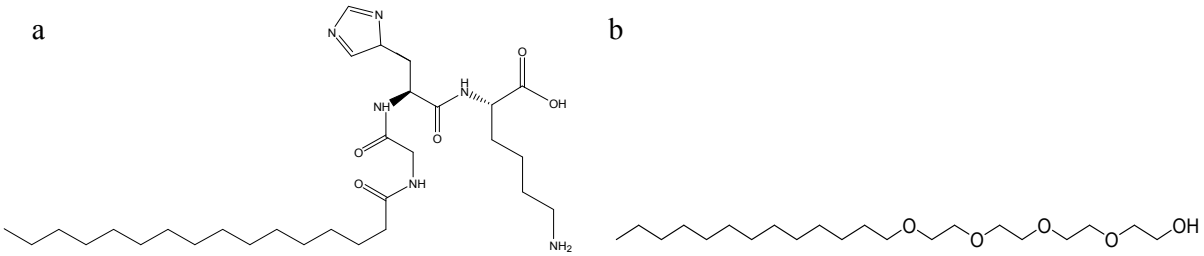

Figure 1. Chemical structures of (a) C_{16}-GK-3 and (b) $C_{12}E_4$ molecules.

Methods and characterization

For transmission electron microscopy (TEM) observations, about 5 μ L of solution was placed on a carbon-coated copper grid (400 mesh) and the excess solution was wicked away with filter paper. The copper grids were freeze-dried and observed on a JEOL JEM-100 CXII (Japan) at an accelerating voltage of 80 kV with a Gatanmultiscan CCD for collecting images. FE-SEM observations were carried out on a JSM-6700F. For atomic force microscopy (AFM) observations, a drop of gel solution was placed on a silica wafer, which was freeze-dried at -60 °C for 12 hours and then observed using Dimension Icon (American) with scan asyst. An SCANASYST-AIR silicon nitride probe was employed.

FT-IR spectrum was recorded on a VERTEX-70/70v spectrometer (Bruker Optics, Germany). Circular dichroism (CD) spectra were obtained using a JASCO J-810 spectropolarimeter, which was

flushed with nitrogen during operation. Wavelength scans were recorded at 0.1 nm intervals from 300 to 180 nm. The hydrogels were determined using a 0.1 mm path length quartz cuvette; the micellar solution used a 1 mm path length quartz cuvette. Small-angle X-ray scattering (SAXS) observations were carried out on a HMBG-SAX X-ray small-angle scattering system (Austria) with a Ni-filtered Cu Kα radiation (0.154 nm) operating at 50 kV and 40 mA. The distance between the sample and detector was 27.8 cm. Polarized microscopy observations were carried out on AXIOSKOP 40/40 FL (ZEISS, Germany) microscope and Nikon Eclipse E400 microscope equipped with a LINKAM THMS 600 heating/cooling stage.

The rheological measurements were carried out on a HAAKE RS75 rheometer with a cone-plate system (Ti, diameter, 35 mm; cone angle, 1°). For the shear-dependent behavior, the viscosity measurements were carried out at shear rates ranging from 0 to 1000 s^{-1}. In oscillatory measurements, an amplitude sweep at a fixed frequency of 1 Hz was performed prior to the following frequency sweep in order to ensure that the selected stress was in the linear viscoelastic region. The viscoelastic properties of the samples were determined by oscillatory measurements in the frequency range of 0.01-10 Hz. The samples were measured at 20.0 ± 0.1 °C with the help of a cyclic water bath.

Results and discussion

Figure 2 shows the phase diagrams of the C_{16}-GK-3/$C_{12}E_4$ system at the fixed concentration of $C_{12}E_4$ (50 g L^{-1}) with increasing the amount of C_{16}-GK-3 (Figure 2 A) and the photos for five typical samples (Figure 2 B-F), respectively. It can be seen that the color of a 50 g L^{-1} solution of $C_{12}E_4$ is translucent. On the addition of C_{16}-GK-3, the sample becomes two phase states (20-40 g L^{-1} added C_{16}-GK-3, the upper phase is translucent and the bottom phase is transparent) and then transfer to a

homogeneous transparent solution, sol and hydrogel states, respectively. This points to a solubilizing effect of the added C_{16}-GK-3, which appears to break up the larger sizes of vesicles of $C_{12}E_4$.

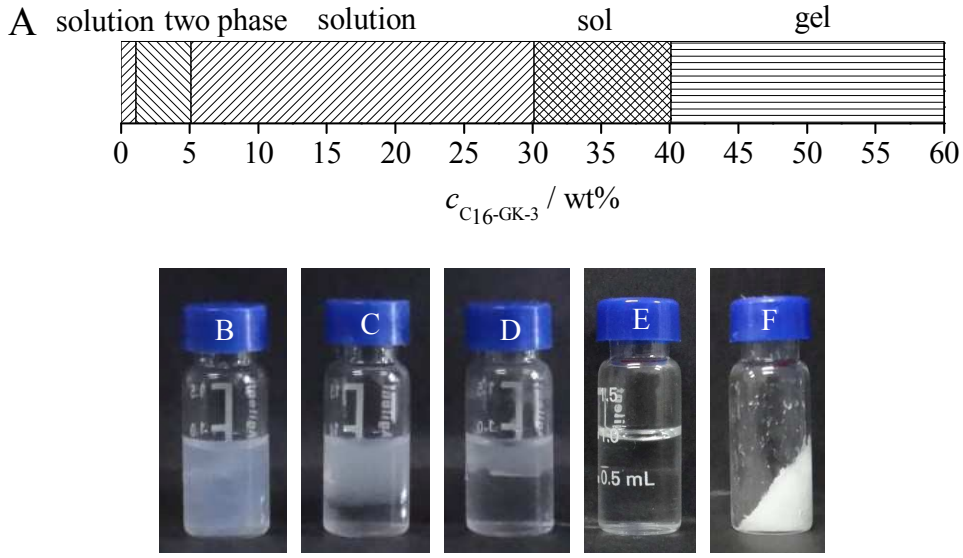

Figure 2 Phase transition with the addition of C_{16}-GK-3 to 50 g L^{-1} $C_{12}E_4$ solutions (A) and sample photographs of typical samples : c_{C12E4} = 50 g L^{-1} and $c_{C16\text{-}GK\text{-}3}$ is changeable: (B) 0, (D) 20, (D) 30, (E) 50, (F) 600 g L^{-1}. T = 20.0 ± 0.1ºC.

Moreover, Figure 3 shows the phase diagrams of the C_{16}-GK-3/$C_{12}E_4$ system at the fixed concentration of C_{16}-GK-3 (50 g L^{-1}) with increasing the amount of $C_{12}E_4$ (Figure 3 A) and the photos for five typical samples (Figure 3 B-F), respectively. It can be seen that the color of a 50 g L^{-1} solution of C_{16}-GK-3 is transparent. Then, the samples transferred to two phase, sol and liquid crystal states, respectively. Phase behavior of more samples investigated was shown in Figure S1 which can give us more information about C_{16}-GK-3/$C_{12}E_4$ mixed system. Thus, through these experimental results, it can be speculated that the rich phase behavior of C_{16}-GK-3/$C_{12}E_4$ mixed system can be adjusted by the composition between the $C_{12}E_4$ and C_{16}-GK-3 and this is the result of the interaction between $C_{12}E_4$ and C_{16}-GK-3.

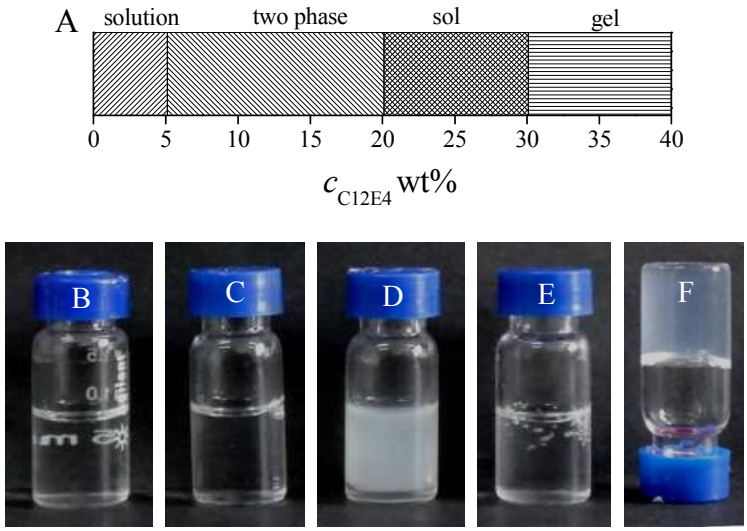

Figure 3 Phase transition with the addition of $C_{12}E_4$ to 50 g L^{-1} C_{16}-GK-3 solutions (A) and sample photographs of typical samples : $c_{C16\text{-}GK\text{-}3}$ = 50 g L^{-1} and c_{C12E4} is changeable: (B) 50, (C) 70, (D) 200, (E) 300, (F) 400 g L^{-1}. T = 20.0 ± 0.1ºC.

Microstructures of the self-assembled aggregates

The microstructures of the self-assembled aggregates were investigated by TEM, FE-SEM and AFM observations. TEM images of the nanostructures formed with constant c_{C12E4} (50 g L^{-1}) and various $c_{C16\text{-}GK\text{-}3}$ are shown in Figure 4. It was clearly seen that incremental additions of C_{16}-GK-3 to $C_{12}E_4$ solution induced a morphological transition in the self-assembled state, ultimately changing from vesicle (Figure 4 A) to globular dandelion-like nanostructures (Figure 4 B, $c_{C16\text{-}GK\text{-}3}$ = 100 g L^{-1}) and then to dendrite structures composed of micron-sized fibers (Figure 4 C and D, $c_{C16\text{-}GK\text{-}3}$ = 200 g L^{-1} and 300 g L^{-1}).

The delicate structure of 50 g L^{-1} C_{16}-GK-3/100 g L^{-1} $C_{12}E_4$ were further characterized by SEM and AFM (Figure 5). The dandelion-like morphology consist of left-handed helical nanotapes (Figure 5 C) and some nanotapes further coiled to form lager-sized superhelix. The appearance of the assemblies showed in AFM images may be more compact than the TEM. It is speculated that

the dandelion-like structures with a relative height of 1.35 μm compared to peripheric surface could contact with the tip, leading the nanotapes at the surface somewhat destroyed and even separated from the assemblies, consequently, the remaining strutures at the surface cannot self-support and collapsed. The AFM images of dendrite structures formed with c_{C12E4} = 50 g L^{-1} and $c_{C16\text{-}GK\text{-}3}$ = 200 g L^{-1} were shown in Figure 6. The assemblies are, exclusively, composed of helical nanotapes with left-handed bias (Figure 5 B), furthermore, some of the nanohelices aggregated into bundles. The measured helical pitches is about 170nm. From the above results, hierarchically self-assembled process can be achieved that helical nanotapes with left handed direction indued by the chirality of peptide molecules were first observed, then, the smaller -sized nanohelices aggregated into larger assemblies. The schematic illustration of the formation of C_{16}-GK-3/$C_{12}E_4$ nanostructure with the increase concentration of C_{16}-GK-3 are shown in Scheme 1.

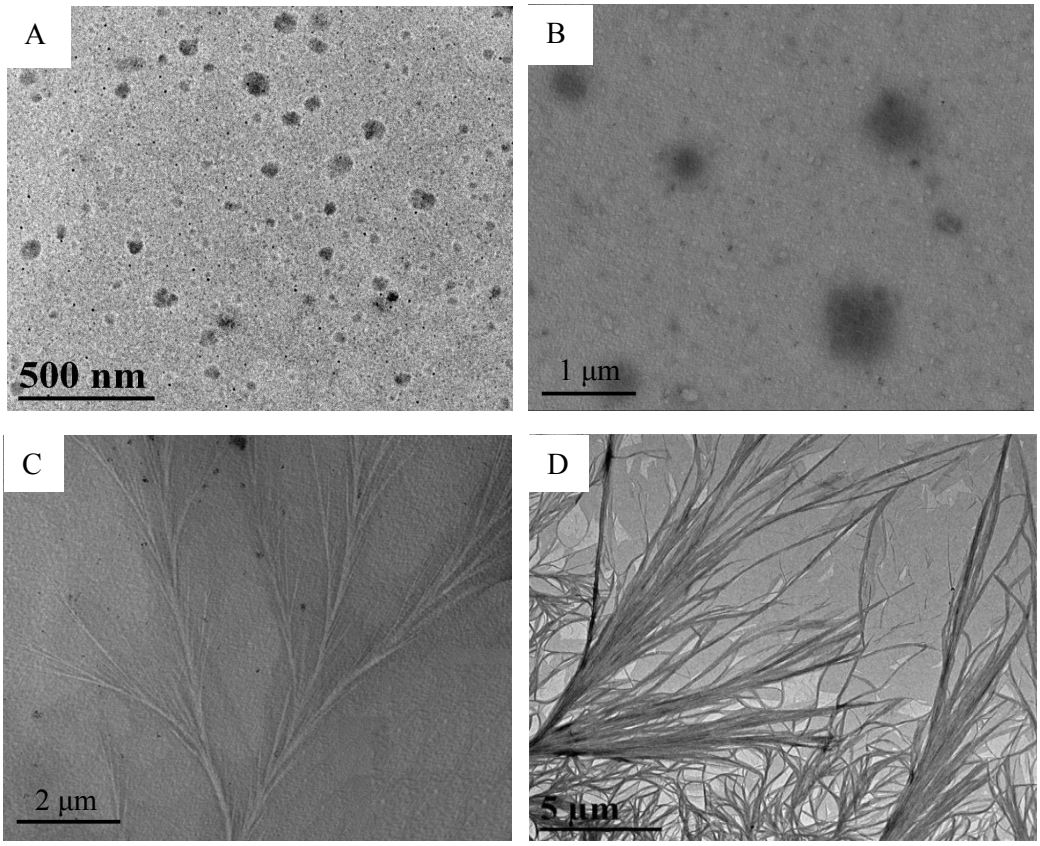

Figure 4 TEM images of the nanostructures formed with constant c_{C12E4} (50 g L^{-1}) and various $c_{C16\text{-}GK\text{-}3}$. (A) 0 g L^{-1} C_{16}-GK-3; (B) 100 g $L^{-1}$$C_{16}$-GK-3; (C) 200 g L^{-1} C_{16}-GK-3; (D) 300 g L^{-1} C_{16}-GK-3.

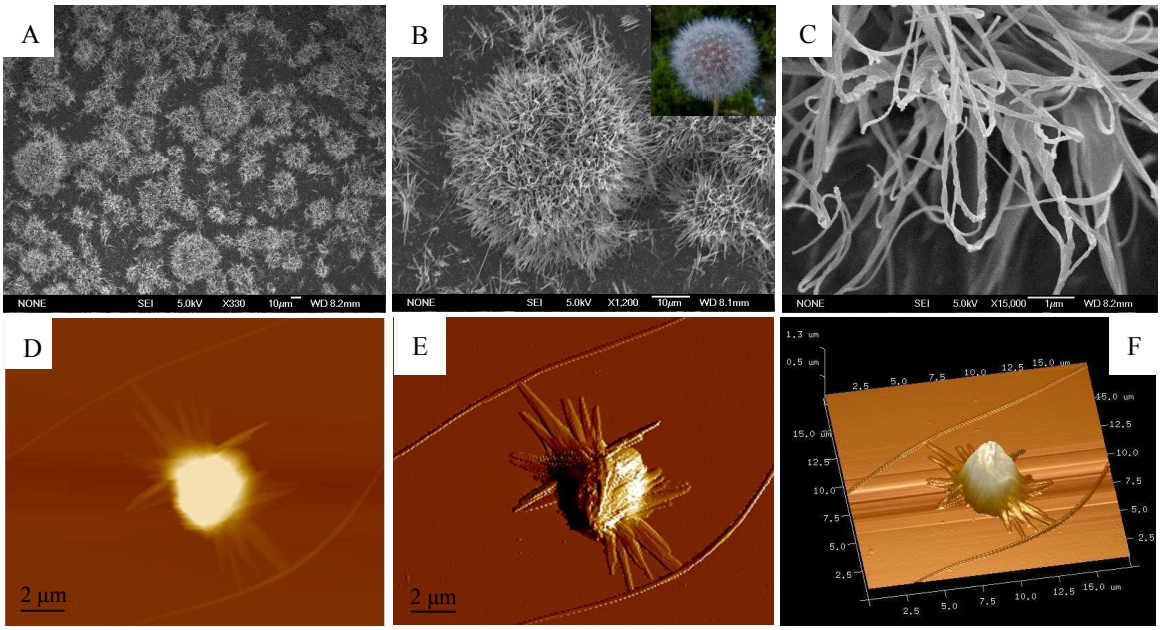

Figure 5 SEM (A, B, C) and AFM (D, E, F) images of the dandelion-like nanostructures formed with c_{C12E4} = 50 g L^{-1} and $c_{C16\text{-}GK\text{-}3}$ = 100 g L^{-1}. A-C: Images were taken under different magnification. Inset of B is the real dandelion photo. D is the AFM height images; E is the AFM peak force images; F is the three-dimensional (3D) morphology of the sample.

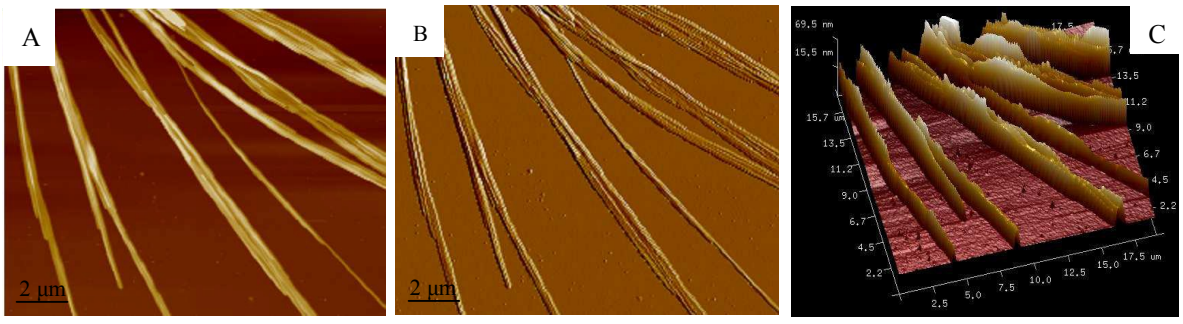

Figure 6 AFM images of the dendrite nanostructures formed with c_{C12E4} = 50 g L^{-1} and $c_{C16\text{-}GK\text{-}3}$ = 200 g L^{-1}. A is the AFM height images; B is the AFM peak force images; C is the three-dimensional (3D) morphology of the sample.

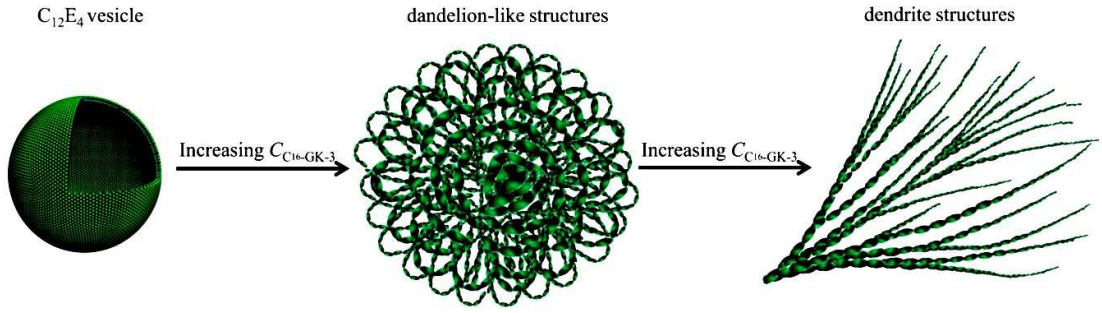

Scheme 1 The schematic illustration of the formation of C_{16}-GK-3/$C_{12}E_4$ nanostructure with the increase concentration of C_{16}-GK-3.

If the concentration of $c_{C16\text{-}GK\text{-}3}$ is fixed at 50 g L^{-1} and the concentration of c_{C12E4} was changed. The microstructures of C_{16}-GK-3/$C_{12}E_4$ mixed system were also changed from vesicle to dendrite structures as shown in Figure 7. If we further increase the concentration of $C_{12}E_4$ to 300 g L^{-1} and 400 g L^{-1}, the sample can form liquid crystal (LC) and it is hard to use TEM to observe its morphology, thus, POM were used to observe its polarized property and the results were shown in Figure 8. It can be seen that for the pure 200 g L^{-1} $C_{12}E_4$, it can not form LC and there is no polarized texture. But when 50 g L^{-1} C_{16}-GK-3 was added, it can form LC and polarized texture can be observed. For 300 g L^{-1} and 400 g L^{-1} $C_{12}E_4$, they are lamellar liquid crystal (LLC) which showed Maltese crosses texture, when 50 g L^{-1} C_{16}-GK-3 was added, although the lamellar structures of the samples were kept, however, it changed into the oil texture, indicating the influence of C_{16}-GK-3 on the properties of $C_{12}E_4$ liquid crystal.

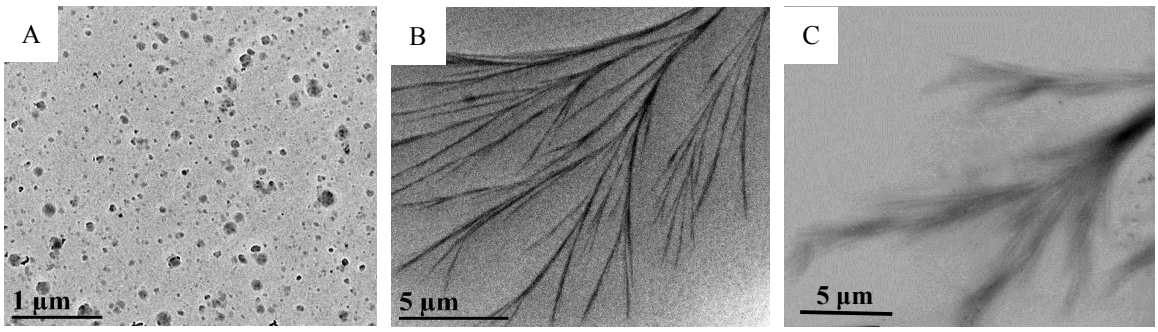

Figure 7 TEM images of the nanostructures formed with constant $c_{C16\text{-}GK\text{-}3}$ (50 g L^{-1}) and various c_{C12E4}: (A) 50 g L^{-1} $C_{12}E_4$; (B) 100 g L^{-1} $C_{12}E_4$; (C) 200 g L^{-1} $C_{12}E_4$.

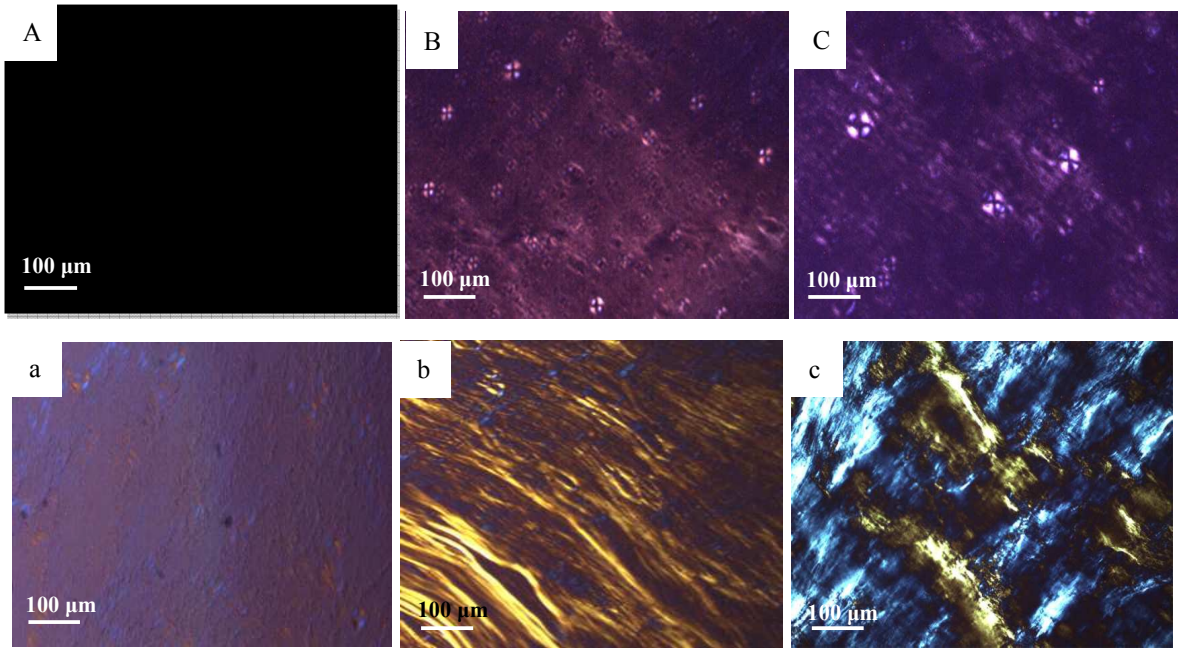

Figure 8 POM images of $C_{12}E_4$ LLC matrix without C_{16}-GK-3: (A) 200 g L^{-1} $C_{12}E_4$, (B) 300 g L^{-1} $C_{12}E_4$, (C) 400 g L^{-1} $C_{12}E_4$. POM image of $C_{12}E_4$ LLC matrix with C_{16}-GK-3: (a) 200 g L^{-1} $C_{12}E_4$/50 g L^{-1} C_{16}-GK-3, (b) 300 g L^{-1} $C_{12}E_4$/50 g L^{-1} C_{16}-GK-3, (c) 400 g L^{-1} $C_{12}E_4$/50 g L^{-1} C_{16}-GK-3.

To further obtain the details about the phase behaviors of C_{16}-GK-3/$C_{12}E_4$ LLC composites, SAXS measurements were carried out. Figure 9 showed the variation of SAXS results of 50 g L^{-1} C_{16}-GK-3 as a function of the concentration of $C_{12}E_4$ (200-400 g L^{-1}). The SAXS results show two scattering peaks, indicative of the highly ordered supramolecular structures. All the ratios of the two peaks are 1 : 2, suggesting a typical lamellar structure of the supra-molecular structures. Moreover, the position of the peaks moved to left a bit with the increasing of $C_{12}E_4$. The d-spacing of the lamellar lattice was calculated by $d = 2\pi/q_1$ (q_1 was the value of the first peak). The calculated inter-planar distances (d) of the typical lamellar structures are 12.1, 9.1, 6.6 nm for 200 g L^{-1} $C_{12}E_4$/50 g L^{-1} C_{16}-GK-3, 300 g L^{-1} $C_{12}E_4$/50 g L^{-1} C_{16}-GK-3, 400 g L^{-1} $C_{12}E_4$/50 g L^{-1} C_{16}-GK-3,

respectively. Compared with the values of d-spacing for the pure 300 g L^{-1} (d = 10.55 nm) and 400 g L^{-1} (d = 8.32 nm) $C_{12}E_4$, it can be seen that the addition of C_{16}-GK-3 made d-spacing of the lamellar lattice decreases which indicated that the molecular arrangement is more closely in C_{16}-GK-3/$C_{12}E_4$ LLC composites.

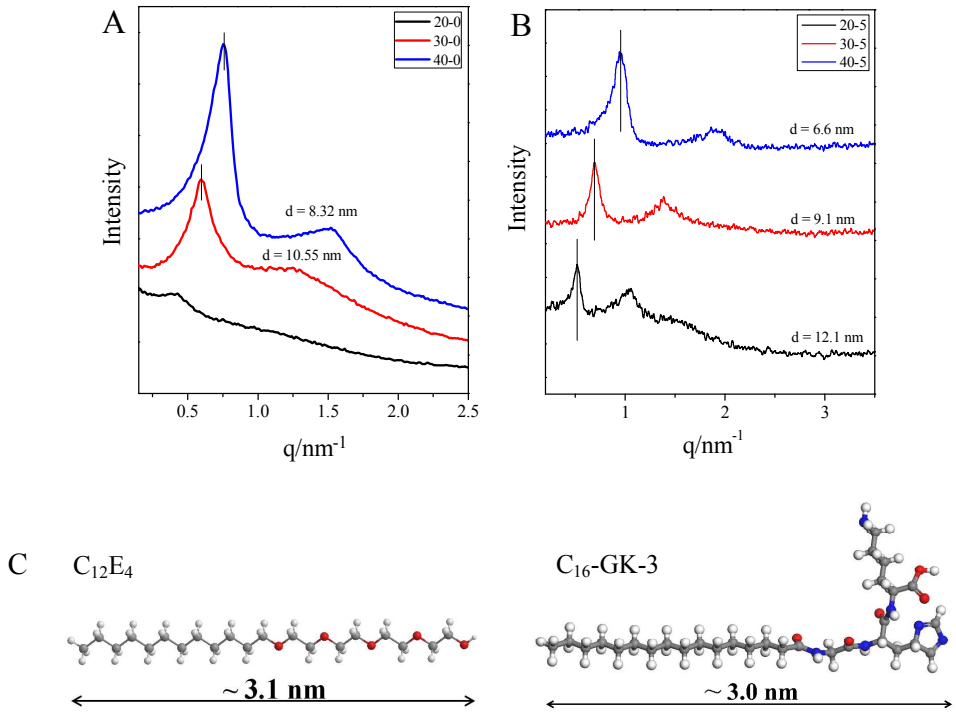

Figure 9 The results of SAXS of (A) pure $C_{12}E_4$ LLC and (B) C_{16}-GK-3/$C_{12}E_4$ LLC composites. (C) The ball-and-stick models (obtained by Material Studio software) of $C_{12}E_4$ and C_{16}-GK-3 molecules. Color code for atoms: blue, nitrogen; red, oxygen; dark gray, carbon; light gray, hydrogen.

Rheological measurements can give macro properties of the system and it is an important method to investigate LLC materials [31-33]. The results of the rheological properties of liquid crystal composites as a function of the concentration of $C_{12}E_4$ when $c_{C16\text{-}GK\text{-}3}$ = 50 g L^{-1} were shown in Figure 10. It can be seen that the increase of c_{C12E4} greatly increased the range of the linear viscoelastic region of LLC phase, and the shear modulus increased with the increase of c_{C12E4}. For example, the elastic modulus (G′) of the weak lamellar phase of 200 g L^{-1} $C_{12}E_4$/50 g L^{-1} C_{16}-GK-3

was 4.7 Pa, and the value of G′ increased progressively from 120 Pa to 413 Pa when c_{C12E4} increased from 30 g L^{-1} to 40 g L^{-1}. For 200 g L^{-1} $C_{12}E_4$/50 g L^{-1} C_{16}-GK-3, G′ and viscous modulus (G″) are slightly dependent of oscillatory frequency with the same values of about 3.4 Pa at f =5 Hz, indicating the weak elasticity. When c_{C12E4} increases to 300 and 400 g L^{-1}, G′ and G″ are nearly independent of oscillatory frequency but increase to 7.49 and 4.87 Pa for 300 g L^{-1} $C_{12}E_4$/50 g L^{-1} C_{16}-GK-3 and 9.11 and 6.03 Pa for 400 g L^{-1} $C_{12}E_4$/50 g L^{-1} C_{16}-GK-3, respectively, exhibiting the obvious viscoelasticity and the elastic dominant property. The η* of both systems decreased with the increase of frequency indicating a shear-thinning behavior (Figure 10 C). Moreover, the value of η* increased with the increase of c_{C12E4} which indicated that the increase of c_{C12E4} enhanced the mechanical property of C_{16}-GK-3/$C_{12}E_4$ LLC composites.

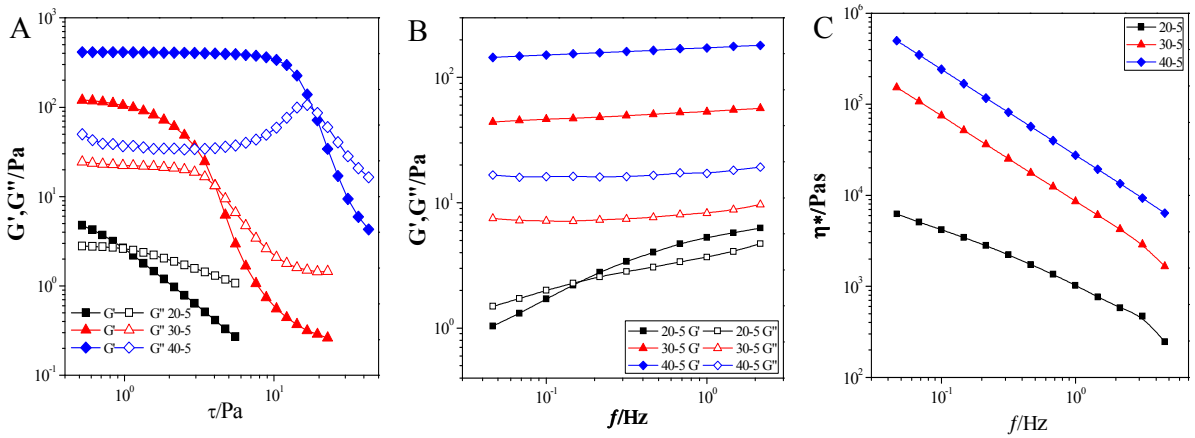

Figure 10 Rheological properties of C_{16}-GK-3/$C_{12}E_4$ LLC composites as a function of the concentration of $C_{12}E_4$ when $c_{C16\text{-}GK\text{-}3}$ = 50 g L^{-1} (A) G′ and G″ as a function of the applied stress (τ) at f = 1.0 Hz, (B) G′ and G″ and (C) η* as a function of f.

To further characterize the features of the formed nanostructures at various concentrations of $C_{12}E_4$ and C_{16}-GK-3, the FTIR and CD spectra were measured, as shown in Figure 11. From the IR spectra, it can be seen that for pure C_{16}-GK-3, no *β*-sheet secondary structure was noticed. The

spectra of the $C_{12}E_4/C_{16}$-GK-3 mixtures, however, changed. The spectra displayed a strong peak at 1619 cm^{-1} which is consistent with the presence of β-sheets and a second one at 1679 cm^{-1} ,which is characteristic of an antiparallel arrangement of the β-sheets [34]. Additional contribution at 1650 cm^{-1} indicates that the peptide region also adopts random coil characteristic [35].The wide peak (~ 3400 cm^{-1}) is well-known for symmetric and antisymmetric O−H stretching modes, the stretching vibration of N-H locates at 3300 cm^{-1} and the peaks at 2920 cm^{-1} and 2852 cm^{-1} are the asymmetric and symmetric stretching vibration of CH_2 of $C_{12}E_4$ and C_{16}-GK-3, respectively. For CD analysis, it can be seen that the pure C_{16}-GK-3 solution lacks characteristic structure, while no CD signals can be observed in micelle solution of $C_{12}E_4$. After the interaction between $C_{12}E_4$ and C_{16}-GK-3, the formation of helical dandelion-like or dendrite structures resulting in a remarkable CD signal (Fig. 8e), β-sheets and random coil structures were proved to coexist from the peaks at 215 and 200 nm confirming the helical structure and higher ordered molecular arrangement of $C_{12}E_4/C_{16}$-GK-3 [36]. It was obvious that the peak for the β-sheets structure was greater than that of the random coil structure, which indicated more β-sheets structure than random coil structure formed in the obtained nanostructures.

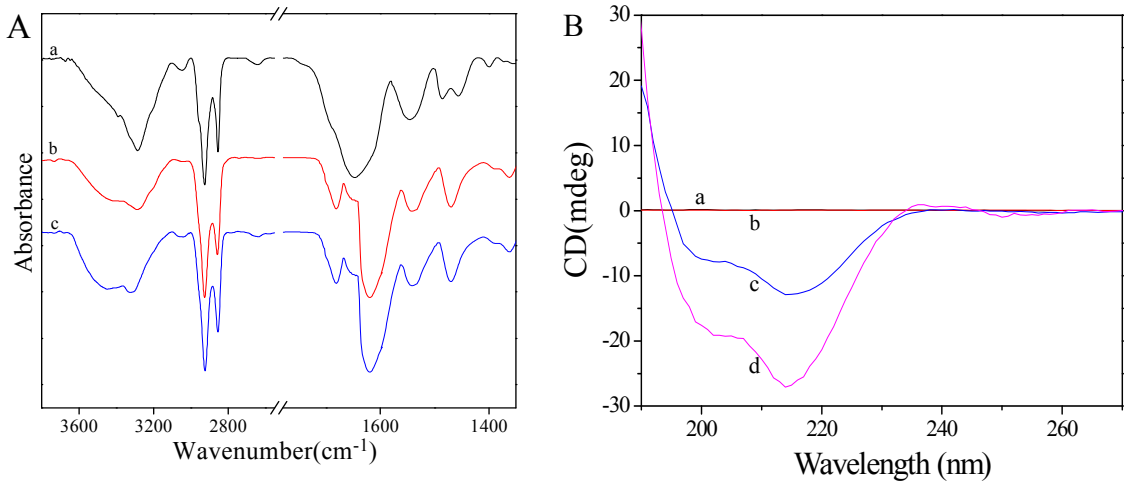

Figure 11 (A) FT-IR spectra of samples: (a) C_{16}-GK-3, (b) 50 g L^{-1} $C_{12}E_4$/100 g L^{-1} C_{16}-GK-3, (c)

50 g L^{-1} $C_{12}E_4$/200 g L^{-1} C_{16}-GK-3. (B) CD spectra of (a) 100 g L^{-1} C_{16}-GK-3, (b) 50 g L^{-1} $C_{12}E_4$, (c) 50 g L^{-1} $C_{12}E_4$/100 g L^{-1} C_{16}-GK-3, (d) 50 g L^{-1} $C_{12}E_4$/200 g L^{-1} C_{16}-GK-3.

Mechanism of the interaction between C_{16}-GK-3 and $C_{12}E_4$

All results above indicate that there is strong interaction between C_{16}-GK-3 and $C_{12}E_4$. Since C_{16}-GK-3 possesses both a hydrophobic tail and many hydrogen-bond sites such as three amide groups and one carboxylic acid, thus, the hydrogen bonding interaction between the amide groups of C_{16}-GK-3 and polyoxyethylene groups of $C_{12}E_4$ and hydrophobic interaction between the alkyl chains of C_{16}-GK-3 and $C_{12}E_4$ during self-assembly led to the formation of the bilayer structure which serve as basic structural units for subsequent hierarchical self-assembly [37]. Due to the chiral nature of C_{16}-GK-3 molecules, the hydrogen bond between the headgroup of C_{16}-GK-3 and $C_{12}E_4$ leads the bilayer structure to roll into the helical fibers. It is suggested that a subtle balance between various hydrogen bonds played an important role for the construction of nanostructures. Incremental additions of C_{16}-GK-3 to $C_{12}E_4$ solution induced the formation of the strong hydrogen bonds between the amide groups of C_{16}-GK-3 and stabilized the bilayer structures which eventually formed dandelion-like and dendrite nanostructures composed of micron-sized helical fibers.

Conclusion

The aggregation behavior of the mixture of a peptide amphiphile (C_{16}-GK-3) and a nonionic surfactant ($C_{12}E_4$) in aqueous solution was systematically investigated by the TEM, HR-TEM, AFM, SAXS, FT-IR, CD and rheological measurements. By fixing the concentration of $C_{12}E_4$ while changing the concentration of C_{16}-GK-3 or fixing the concentration of C_{16}-GK-3 while increasing concentration the concentration of $C_{12}E_4$, the transitions from solution, two phase, sol to hydrogel

state were obtained, the hierarchically self-assembled process was observed that left-handed nanofibers induced by the chirality of peptide molecules were first formed, the nanohelices, then, aggregated into larger dandelion-like and dendrite nanostructures. The assembly process was driven by the hydrophobic interactions of the alkyl chains, hydrogen bonding interaction between the headgroups of C_{16}-GK-3 and between C_{16}-GK-3 and $C_{12}E_4$. Understanding of the self-assembled supramolecular structures not only offers insights into how rationally designed chiral nanostructures from simple peptide building blocks but also is of significant practical value for the development of the studies both biological and chemical.

Acknowledgement

We gratefully acknowledge financial support from the National Natural Science Foundation of China (21573130, 21173128, 21203109) and the Natural Science Foundation for Distinguished Young Scholars of Shandong Province (JQ201303).

References

1. X. Zhao, F. Pan, H. Xu, M. Yaseen, H. Shan, C. A. Hauser, S. Zhang and J. R. Lu, Chemical Society Reviews, 2010, 39, 3480-3498.

2. H. Cui, M. J. Webber and S. I. Stupp, Peptide Science, 2010, 94, 1-18.

3. J. B. Matson, R. H. Zha and S. I. Stupp, Current Opinion in Solid State and Materials Science, 2011, 15, 225-235.

4. J. Liu and X. Zhao, Nanomedicine, 2011, 6, 1621-1643.

5. H. Guo, J. Zhang, T. Xu, Z. Zhang, J. Yao and Z. Shao, Biomacromolecules, 2013, 14, 2733-2738.

6. A. Dehsorkhi, V. Castelletto and I. W. Hamley, Journal of Peptide Science, 2014, 20, 453-467.

7. D. W. Löwik and J. C. van Hest, Chemical Society Reviews, 2004, 33, 234-245.

8. V. Castelletto, I. Hamley, M. Segarra-Maset, C. B. Gumbau, J. Miravet, B. Escuder, J. Seitsonen and J. Ruokolainen, Biomacromolecules, 2014, 15, 591-598.

9. I. W. Fu, C. B. Markegard, B. K. Chu and H. D. Nguyen, Advanced healthcare materials, 2013, 2, 1388-1400.

10. H. Xu, Y. Wang, X. Ge, S. Han, S. Wang, P. Zhou, H. Shan, X. Zhao and J. R. Lu, Chemistry of Materials, 2010, 22, 5165-5173.

11. J. B. Matson and S. I. Stupp, Chemical Communications, 2012, 48, 26-33.

12. Y. Li, B. Li, Y. Fu, S. Lin and Y. Yang, Langmuir, 2013, 29, 9721-9726.

13. E. Kokkoli, A. Mardilovich, A. Wedekind, E. L. Rexeisen, A. Garg and J. A. Craig, Soft Matter, 2006, 2, 1015-1024.

14. F. Versluis, H. R. Marsden and A. Kros, Chemical Society Reviews, 2010, 39, 3434-3444.

15. H. Cui, T. Muraoka, A. G. Cheetham and S. I. Stupp, Nano letters, 2009, 9, 945-951.

16. H. A. Behanna, J. J. Donners, A. C. Gordon and S. I. Stupp, Journal of the American Chemical Society, 2005, 127, 1193-1200.

17. Y. Fu, B. Li, Z. Huang, Y. Li and Y. Yang, Langmuir, 2013, 29, 6013-6017.

18. S. E. Paramonov, H.-W. Jun and J. D. Hartgerink, Journal of the American Chemical Society, 2006, 128, 7291-7298.

19. W. T. Truong, Y. Su, J. T. Meijer, P. Thordarson and F. Braet, Chemistry, an Asian journal, 2011, 6, 30-42.

20. M. J. Webber, J. Tongers, M.-A. Renault, J. G. Roncalli, D. W. Losordo and S. I. Stupp, Acta

biomaterialia, 2010, 6, 3-11.

21. A. Mata, Y. Geng, K. J. Henrikson, C. Aparicio, S. R. Stock, R. L. Satcher and S. I. Stupp, Biomaterials, 2010, 31, 6004-6012.

22. P. Palladino, V. Castelletto, A. Dehsorkhi, D. Stetsenko and I. W. Hamley, Langmuir, 2012, 28, 12209-12215.

23. L. W. Chow, L.-j. Wang, D. B. Kaufman and S. I. Stupp, Biomaterials, 2010, 31, 6154-6161.

24. M. N. Melo, R. Ferre and M. A. Castanho, Nature Reviews Microbiology, 2009, 7, 245-250.

25. I. Hamley, Soft Matter, 2011, 7, 4122-4138.

26. V. Castelletto, I. W. Hamley, J. Perez, L. Abezgauz and D. Danino, Chemical Communications, 2010, 46, 9185-9187.

27. D. W. Löwik, J. Garcia-Hartjes, J. T. Meijer and J. C. van Hest, Langmuir, 2005, 21, 524-526.

28. T. Otsuka, T. Maeda and A. Hotta, The Journal of Physical Chemistry B, 2014, 118, 11537-11545.

29. A. Dehsorkhi, V. Castelletto, I. Hamley and P. Lindner, Soft Matter, 2012, 8, 8608-8615.

30. V. Castelletto, I. W. Hamley, J. Adamcik, R. Mezzenga and J. Gummel, Soft Matter, 2012, 8, 217-226.

31. A. Babaei and A. Arefazar, Journal of Applied Polymer Science, 2015, 132.

32. R. Bhargavi, G. G. Nair, S. K. Prasad, R. Majumdar and B. G. Bag, Journal of Applied Physics, 2014, 116, 154902.

33. L. Wang, X. Xin, M. Yang, J. Shen and S. Yuan, RSC Advances, 2015, 5, 68404-68412.

34. I. W. Hamley, M. J. Krysmann, A. Kelarakis, V. Castelletto, L. Noirez, R. A. Hule and D. J. Pochan, Chemistry-A European Journal, 2008, 14, 11369-11375.

35. V. Castelletto, I. W. Hamley, J. Adamcik, R. Mezzenga and J. Gummel, Soft Matter, 2012, 8, 217-226.

36. T. Koga, M. Matsuoka and N. Higashi, Journal of the American Chemical Society, 2005, 127, 17596-17597.

37. P. Duan, L. Qin, X. Zhu and M. Liu, Chemistry-A European Journal, 2011, 17, 6389-6395.